Journal of Power Sources 233 (2013) 304–308

Contents lists available at SciVerse ScienceDirect

Journal of Power Sources

journal homepage: www.elsevier.com/locate/jpowsour

Short communication

Facile synthesis of belt-like $Ag_{1.2}V_3O_8$ with excellent stability for rechargeable lithium batteries

Shuquan Liang, Tao Chen, Anqiang Pan*, Jiang Zhou, Yan Tang, Ruomei Wu

School of Materials Science and Engineering, Central South University, Changsha 410083, China

HIGHLIGHTS

- $Ag_{1.2}V_3O_8$ nanobelts have been fabricated by a facile solid-state approach.
- The morphology and the purity of $Ag_{1.2}V_3O_8$ are largely temperature-dependent.
- The $Ag_{1.2}V_3O_8$ nanobelts electrodes have good cyclability and rate capability.

ARTICLE INFO

Article history:
Received 29 September 2012
Received in revised form
31 December 2012
Accepted 19 January 2013
Available online 28 January 2013

Keywords:
Silver vanadium oxide
Nanobelt
Lithium ion batteries
Temperature-dependent

ABSTRACT

Silver vanadium oxide ($Ag_{1.2}V_3O_8$) has been successfully synthesized by a facile solid-state reaction between $AgNO_3$ and sol–gel prepared VOC_2O_4. The morphology and phase of the calcinations products are largely temperature-dependent. The morphologies of the calcinations products evolutes from nanorods to nanobelts and higher purity can be obtained with the raise of temperatures. Nanobelts with a thickness around 200 nm can be obtained at 450 °C. The as-synthesized $Ag_{1.2}V_3O_8$ nanobelts are of single crystal. As a cathode material for rechargeable lithium ion batteries, the $Ag_{1.2}V_3O_8$ nanobelts exhibit good cyclic stability and high-rate capability. A stable specific discharge capacities of 215, 198, and 174 mA h g^{-1} can be delivered at the current densities of 50, 100 and 200 mA g^{-1}, respectively. The superior performances are attributed to the good reversibility of electrochemically formed LiV_3O_8 and improved conductivity by in-situ formed Ag phase.

1. Introduction

Because of the high specific discharge capacity, high-rate capability and long-term stability [1–4], lithium/silver vanadium oxides (Li/SVOs) as primary batteries have reached great commercial success [5–7]. Up till now, many strategies, such as sol–gel method [8], rheological phase reaction method [1], hydrothermal process [7], ultrasonic irradiation [9], ion-exchange reaction [10] and the conventional solid-state method [11,12] have been employed to fabricate silver vanadium oxides (SVOs) with different Ag–V ratios ($Ag_2V_4O_{11}$, β-$AgVO_3$, etc.). However, the SVOs prepared by these methods can only be applied for high-power non-rechargeable lithium batteries because of the irreversible structural changes during lithium intercalation/de-intercalation process [3,4]. Great efforts have been devoted to increase their electrochemical performances including reducing the particle size, modifying the surface and increasing the crystallinity [2,6,11]. However, it is still a big challenge to obtain SVOs electrodes with long cyclic stability, high capacity and rate capability.

$Ag_{1+x}V_3O_8$ is isostructural to $Li_{1+x}V_3O_8$ and is composed of $(V_3O_8)^{n-}$ layers, which retains its layered structures during discharge/charge process [5,6]. The good structural stability may ensure better cycling performance, especially compared to other silver oxides (such as $AgVO_3$ and $Ag_2V_4O_{11}$) which lose their integrity during cycling [13–16]. However, the usage of $Ag_{1+x}V_3O_8$ as a secondary cathode material is rarely reported. Recently, the morphologies of the active materials have been reported to have a big effect to their electrochemical performance. In particular, nanomaterials have been widely used in lithium ion batteries because of their advantages in lower polarization, shorter Li^+ ions diffusion distance and higher utilization rate of active materials than their bulk counterpart [17–19]. Among the various methods reported for the synthesis of nanomaterials, solid-state reaction is believed to be the most cost-effective and easy to scale up approach [20–22].

Herein, we report the facile synthesis of novel $Ag_{1.2}V_3O_8$ nanobelts through a solid-state reaction between $AgNO_3$ and VOC_2O_4.

* Corresponding author. Tel.: +86 0731 88836069; fax: +86 0731 88876692.
E-mail address: pananqiang@gmail.com (A. Pan).

0378-7753/$ – see front matter © 2013 Elsevier B.V. All rights reserved.
http://dx.doi.org/10.1016/j.jpowsour.2013.01.129

The VOC_2O_4 is prepared by a sol–gel process from oxalic acid and V_2O_5 powder. The temperature-dependent morphology and phase transition have been studied. As cathode materials for rechargeable lithium ion batteries, they exhibit excellent cyclic stability and rate capability. The cycling performance is much improved when compared to other silver vanadium oxides.

2. Experimental section

Vanadyl oxalate (VOC_2O_4) was used as vanadium source and was prepared similarly to our early reports [20,23,24]. In brief, V_2O_5 and $H_2C_2O_4{\cdot}2H_2O$ in a molar ratio of 1:3 were added into distilled water, followed by stirring at 80 °C for several hours until the formation of clear blue solution. A stoichiometric amount of $AgNO_3$ was then added into the blue solution under stirring for another 30 min. The mixture solution was dried at 80 °C overnight in an electrical oven. The as-obtained precursor was calcined at 400 °C, 450 °C and 500 °C in air for 2 h and the obtained products were designated as Ag400, Ag450 and Ag500, respectively.

The calcinations process of the precursor was characterized by thermogravimetric analysis (TG) and differential scanning calorimetry (DSC) experiments in air at a heating rate of 10 °C min^{-1}. The crystallinity and phases of the prepared samples were determined by X-ray diffraction (XRD, Rigaku D/max2500 XRD with Cu Kα radiation, $\lambda = 1.54178$Å). All the samples were scanned in the range between 10° and 70° with a scan rate of 8° min^{-1}. The morphologies and structural characterization were conducted on a scanning electron microscopy (SEM, FEI Sirion200) and transmission electron microscopy (TEM, HEM–2100F/UHR).

$Ag_{1.2}V_3O_8$, acetylene black and polyvinylidene fluoride (PVDF) binder in a weight ratio of 70:20:10 were mixed and dispersed in *N*-methyl-2-pyrrolidone (NMP) solution to make the slurry. The slurry was coated on aluminum foil and then dried in a vacuum oven at 100 °C for 10 h prior coin-cell assembling. The Li/$Ag_{1.2}V_3O_8$ cells (2016 type coin cells) were assembled in a glove box (Mbraun, Germany) filled with ultra-high purity argon using polypropylene membrane as the separator, Li metal as the anode, and 1-M $LiPF_6$ in ethylene carbonate/dimethyl carbonate (EC/DMC) (1:1 v/v) as the electrolyte. The cyclic voltammetry (CV) curves were obtained on the CHI 660C (CH Instrument Electrochemical workstation). The AC impedance spectroscopy was tested by IM6ex (ZAHNER elektrik, Germany). The cycling performance of the $Ag_{1.2}V_3O_8$ was tested on a Land Battery Tester (Land CT 2001A, Wuhan, China) in the voltage range of 1.5–3.5 V (vs. Li/Li^+).

3. Results and discussion

The formation process of $Ag_{1.2}V_3O_8$ material is characterized by TG and DSC and the results are shown in Fig. 1a. The precursor mixture composed of $AgNO_3$ and VOC_2O_4 powder was calcined in air at a ramping rate of 10 °C min^{-1}. Three distinct stages have been observed on the TG curve. The slow weight loss from 50 °C to 210 °C is attributed to the evaporation of the physically absorbed and chemically bonded water in the precursor mixture. The dramatic weight loss on TG curve and a corresponding exothermal peak at 300 °C on the DSC curve are detected, which can be ascribed to the decomposition of the mixture powders and the generation of heat. The slight weight increase between 345 °C and 528 °C suggests the trapping of oxygen through the oxidation of vanadium. The shrill endothermic peak at 547 °C may be caused by the melting of $Ag_{1.2}V_3O_8$.

Fig. 1b shows the XRD patterns of the calcinations products obtained at different temperatures. The main diffraction peaks of $Ag_{1.2}V_3O_8$ are detected for Ag400 electrode. However, many impurity phases are observed, which indicates the incompletely

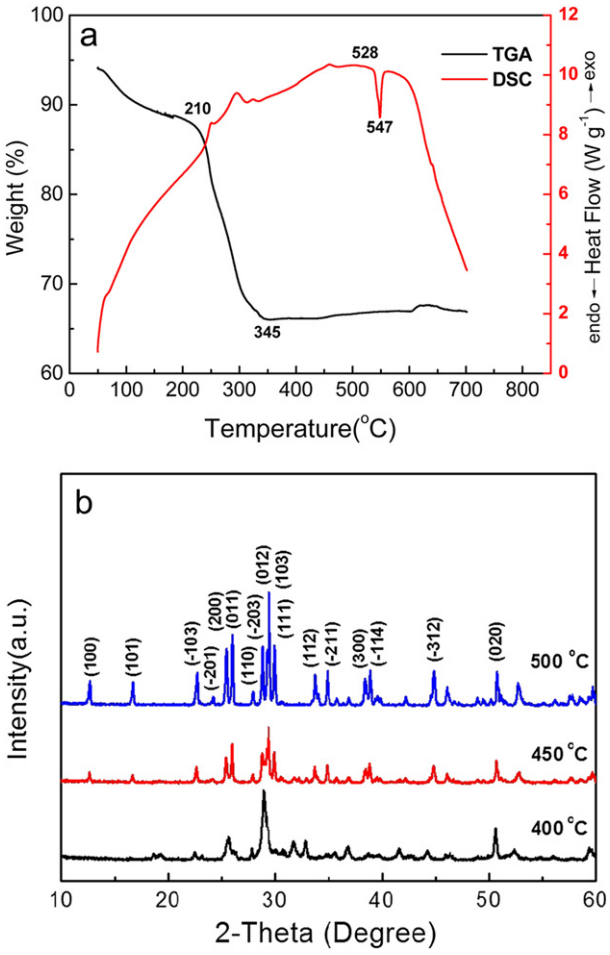

Fig. 1. (a) TG and DSC results for precursor mixture, composed of $AgNO_3$ and VOC_2O_4, calcined in air at a ramping rate of 10 °C min^{-1} (b) XRD patterns of annealing products obtained at different constant temperatures (400 °C, 450 °C and 500 °C) for 2 h.

transformation to $Ag_{1.2}V_3O_8$. $Ag_{1.2}V_3O_8$ with higher purity can be obtained at 450 °C and the XRD pattern matches well to the monoclinic $Ag_{1.2}V_3O_8$ phase (space group: $P2_1/m$ *(11)*, JCPDS card 88-0686, $a = 7.382$, $b = 3.603$, $c = 12.193$). No impurity phase is detected. The result demonstrates the precursor has been fully converted to $Ag_{1.2}V_3O_8$ at 450 °C. As shown in Fig. 1b, $Ag_{1.2}V_3O_8$ with higher crystallinity can be synthesized at 500 °C.

The morphologies of the calcinations products are characterized and the results are shown in Fig. 2. As shown in Fig. 2a, both rod- and belt-like particles are clearly observed for Ag400 electrode. The small nanorods are about 100 nm in width. Moreover, the thickness of the nanobelts is less than 200 nm and the length of which can be several micrometers. As shown in Fig. 1b, the $Ag_{1.2}V_3O_8$ synthesized at 400 °C is accompanied with impurity phases. The formation of the inhomogeneous morphology may be attributed to the incomplete transformation of impurity phase to $Ag_{1.2}V_3O_8$, and thus results in different morphologies. Fig. 2b shows SEM image of $Ag_{1.2}V_3O_8$ material obtained after annealing at 450 °C for 2 h. More uniform nanobelts are exhibited with the thickness ca. 200 nm. No small nanorods are detected. The morphology change suggests the growth of the nanobelts at the expense of the small nanorods at elevated temperatures. Even larger belt-like particles are obtained for Ag500 electrode with the main thickness of 500 nm. As revealed by high-resolution transmission electron microscope (HRTEM) and selected area electron diffractions (SAED) (Fig. 2d), the nanobelt is

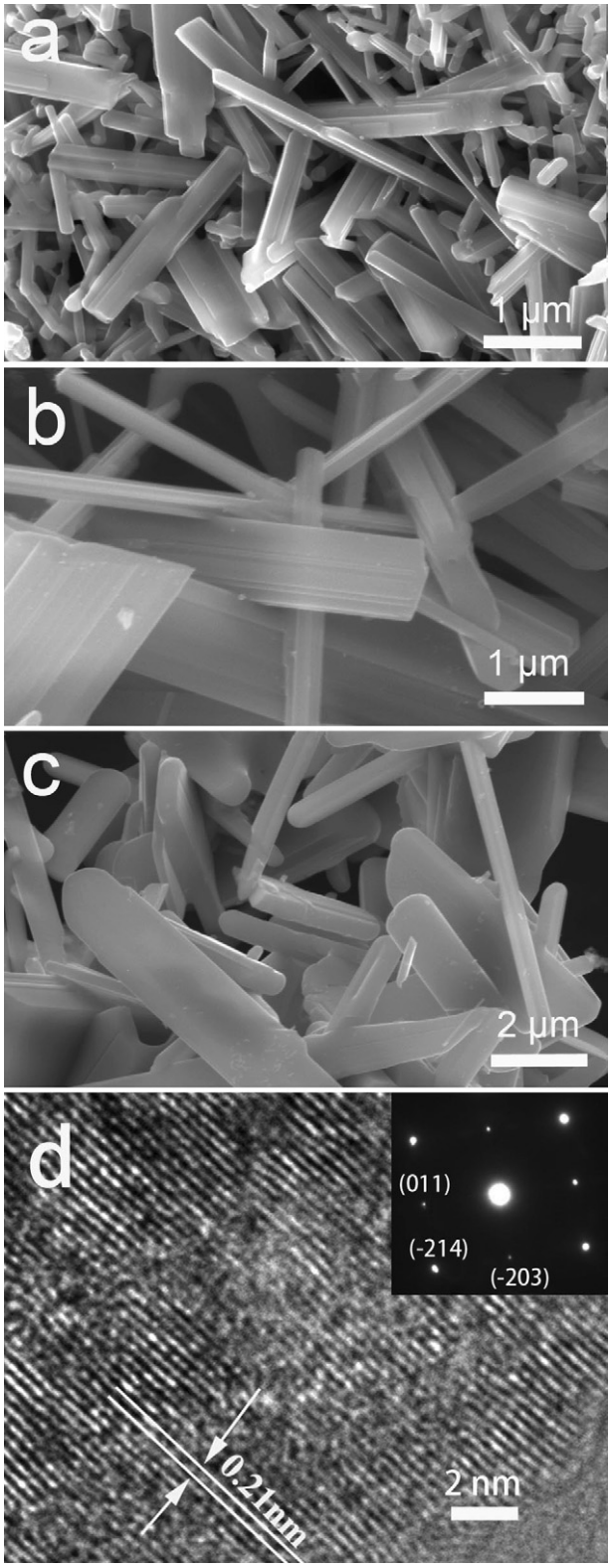

Fig. 2. SEM images of the annealed products: (a) Ag400, (b) Ag450 and (c) Ag500; TEM image (d) and selected area electron diffraction (insets) for Ag500.

a single crystal. The measured distance of 0.21 nm corresponds well with the lattice space of (−214) faces, which indicates the preferential growth direction of the nanobelt approximately along [−214].

Fig. 3 shows four consecutive CV curves of Ag500 electrode in the voltage range of 1.5–3.5 V (vs. Li/Li^+) at a scan rate of 0.1 mV s^{-1}. Only one obvious broad peak at 2.44 V can be identified. More cathodic peaks are observed for the second cycle. This phenomenon may be attributed to the improved reactivity of the electrode materials during cycling. Two cathodic peaks near 2.69 and 2.49 V are attributed to Li^+ ions insertion into the two respective sites with different stabilization energies, and their corresponding anodic peak is shown at 2.8 V [10]. The broad cathodic peak around 2.2 V is related to lithium insertion into a defect rock-salt type structure after phase transition to $Li_4V_3O_8$ and the anodic peak at 2.4 V is only observed for $Li_{1+x}V_3O_8$ type oxides [10,20,25]. Fig. 3b shows the XRD patterns of the cathode material before cycling, after one and five discharge/charge cycling. It is evidenced that the $Ag_{1.2}V_3O_8$ has been converted to LiV_3O_8 and Ag phase after first cycle. Moreover, the LiV_3O_8 phase is recovered after 5 cycles, which indicates the good structural stability of the electrochemical formed LiV_3O_8 upon cycling. However, the metallic silver formed by reduction of Ag(I) at the first cycle is unrecoverable to form $Ag_{1.2}V_3O_8$. This result corresponds to the CV curves, which shows the current density in the anodic peak near 2.8 V was almost constant and no corresponding anodic peaks for Ag(0)–Ag(I) shown over 3.0 V at the first cycles [5,10,26]. Both the identical CV curves for the third and fourth

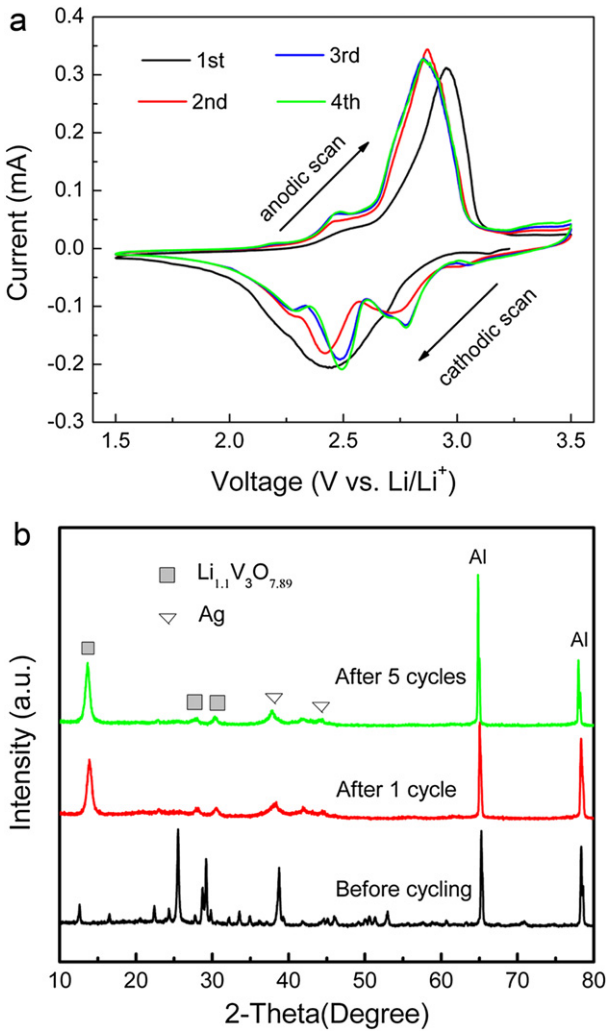

Fig. 3. (a) The first four consecutive cyclic voltammetry (CV) curves for Ag500 electrode at a scan rate of 0.2 mV s^{-1} and (b) XRD patterns for Ag500 electrodes before cycling, after 1 and 5 cycles.

cycles and the XRD patterns indicate the good structural stability of LiV_3O_8.

The electrochemical performances of the silver vanadium oxides (Ag400, Ag450 and Ag500) have been evaluated and the results are shown in Fig. 4. Fig. 4a shows the discharge profiles of the selected cycles for the Ag500 electrode. An initial discharge capacities of 128 mA h g^{-1} can be delivered at a current density of 100 mA g^{-1} and only a broad plateau is observed. The capacity increases upon cycling and reaches a stable specific discharge capacity of 197 mA h g^{-1} at 50th cycle. Moreover, typical plateaus of LiV_3O_8 electrodes are presented. The overlap of the discharge curves for the 50th and the 80th cycles indicates the good stability of the as-synthesized Ag500 electrode. Fig. 4b shows the Nyquist plot of Ag500 electrode measured at the voltage of 3.5 V. A resistance of 800 Ω is detected for $Ag_{1.2}V_3O_8$ electrode, which is much larger than 120 Ω measured after 5 cycles. The lower resistance indicates the improved charge transfer after cycling, which may be caused by the unrecoverable de-intercalated Ag^+ ions and their location on the surface of the electrode materials. Initial discharge capacities of 159, 153, 128 mA h g^{-1} can be delivered for the Ag400, Ag450 and Ag500 electrodes, respectively, under a current density of 100 mA g^{-1}. The higher initial discharge capacity for Ag400 electrode can be attributed to the smaller particles. As shown in Fig. 2, the nanorods are much smaller than the nanobelts. Although higher capacity is delivered for the nanorod-structured Ag400 electrode, its cycling performance is worse than the other electrodes. As shown in Fig. 1b, $Ag_{1.2}V_3O_8$ materials with high purity are synthesized at 450 °C and 500 °C, which would be beneficial to obtain good cycling properties. To our knowledge, $Ag_{1.2}V_3O_8$ electrode with good cyclic stability is first-time reported as cathode material for rechargeable lithium ion batteries. The advantages of $Ag_{1.2}V_3O_8$ over other silver vanadium oxides can be attributed to the stable crystal structures during lithium ions intercalation and de-intercalation. As $Ag_{1+x}V_3O_8$ is isostructural to $Li_{1+x}V_3O_8$, it can retain its $(V_3O_8)^{n-}$ layered structures. The $(V_3O_8)^{n-}$ framework is built up around three crystallographically independent vanadium sites: two octahedrally coordinated and one trigonal-bipyramidal coordination [5,10]. The Ag^+ ions mainly reside in weakly distorted octahedral sites, which correspond to the main Li^+ ion sites observed in $Li_{1.2}V_3O_8$. During the discharge process, Ag^+ is reduced to metallic silver and attaches on the surface of active materials. The $[V_3O_8]^{n-}$ layered structure does not change and thus allows the good structural stability during the discharge/charge process. As shown in Fig. 4c, the capacity of Ag450 electrode is very stable upon cycling, while the capacity for Ag500 electrode keeps increasing in the first 50 cycles and becomes very stable thereafter. This result can be attributed to their morphology-dependent kinetics difference. The thickness of the nanobelt is about 200 and 500 nm for Ag450 and Ag500 electrodes, respectively. The thinner nanobelts can allow the easier Li^+ ions intercalation/de-intercalation into/from the electrodes. However, the capacity of Ag500 electrodes is larger than that of Ag450 after about 30 cycles. The higher capacity for Ag500 electrode makes Ag500 electrode advantage over Ag450 electrode (Fig. 2). This result indicates the capacity and the cycling performance of $Ag_{1.2}V_3O_8$ can be tuned by increasing the crystallinity of $Ag_{1+x}V_3O_8$ electrode and controlling their grain size growth during fabrication process. A specific discharge capacity of 198 mA h g^{-1} can be obtained for Ag500 electrode after 80 cycles at the current density of 100 mA g^{-1}. The cycling behavior of Ag500 electrode at different current densities also has been studied and the results are shown in Fig. 4d. The continuous capacity increase is all detected under different current densities. It should be mentioned that the phenomenon is quite different to the continuous capacity fading for other silver vanadium oxides [2,27]. The good structural reversibility of the electrochemically formed LiV_3O_8 from $Ag_{1.2}V_3O_8$ and the conductivity improvement by reduced Ag phase

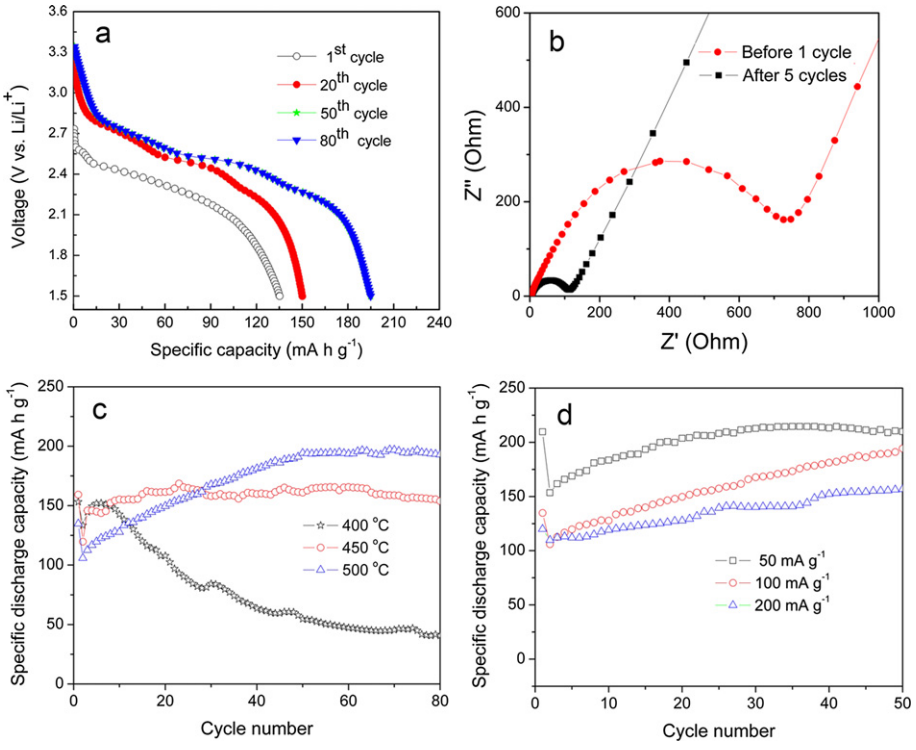

Fig. 4. (a) Discharge curves of the 1st, 20th, 50th and 80th cycle for the Ag500 electrode at a current density of 100 mA g^{-1}. (b) Nyquist plot for Ag500 electrode before cycling and after 5 cycles; (c) cycling behavior of Ag400, Ag450 and Ag500 at the current density of 100 mA g^{-1}; (c) cycling performance of Ag500 electrode under the current densities of 50, 100 and 200 mA g^{-1}. The voltage range for the cycling is from 1.5 to 3.5 V vs. Li/Li^+.

are the main reasons for the capacity increase. A stabilized specific discharge capacities of 215, 198, and 174 mA h g^{-1} can be obtained at the current densities of 50, 100 and 200 mA g^{-1}, respectively. The results demonstrate the as-fabricated $Ag_{1.2}V_3O_8$ nanobelt electrodes with good rate capability and cycling performance are potential cathode materials for rechargeable lithium ion batteries.

4. Conclusions

A facile solid-state method has been developed to fabricate $Ag_{1.2}V_3O_8$ cathode material for rechargeable lithium ion batteries. The annealing temperatures have a great effect on the $Ag_{1.2}V_3O_8$ nanobelts. As a cathode material, $Ag_{1.2}V_3O_8$ electrodes exhibit good cyclic stability and rate capability. The superior electrochemical performance to other silver vanadium oxides suggests the potential application as cathode materials for rechargeable lithium ion batteries.

Acknowledgment

The financial support is provided by Creative Research Group of National Natural Science Foundation of China (Grant No. 50721003) and Lie Ying Program of Central South University.

References

[1] X.Y. Cao, H. Zhan, J.G. Xie, Y.H. Zhou, Mater. Lett. 60 (2006) 435–438.
[2] L.Q. Mai, X. Xu, C.H. Han, Y.Z. Luo, L. Xu, Y.M.A. Wu, Y.L. Zhao, Nano Lett. 11 (2011) 4992–4996.
[3] P.M. Skarstad, J. Power Sourc. 136 (2004) 263–267.
[4] K. West, A.M. Crespi, J. Power Sourc. 54 (1995) 334–337.
[5] P. Rozier, J. Galy, J. Solid State Chem. 134 (1997) 294–301.
[6] K.J. Takeuchi, A.C. Marschilok, S.M. Davis, R.A. Leising, E.S. Takeuchi, Coord. Chem. Rev. 219 (2001) 283–310.
[7] S.Y. Zhang, W.Y. Li, C.S. Li, J. Chen, J. Phys. Chem. B 110 (2006) 24855–24863.
[8] E.S. Takeuchi, A.C. Marschilok, R.A. Leising, K.J. Takeuchi, J. Power Sourc. 174 (2007) 552–553.
[9] J.G. Xie, X.Y. Cao, J.X. Li, H. Zhan, Y.Y. Xia, Y.H. Zhou, Ultrason. Sonochem. 12 (2005) 289–293.
[10] J. Kawakita, Y. Katayama, T. Miura, T. Kishi, Solid State Ionics 99 (1997) 71–78.
[11] R.A. Leising, E.S. Takeuchi, Chem. Mater. 5 (1993) 738–742.
[12] E.S. Takeuchi, P. Piliero, J. Power Sourc. 21–22 (1987) 133–141.
[13] S.Q. Liang, J. Zhou, A.Q. Pan, Y.J. Li, T. Chen, Z.M. Tian, H.B. Ding, Mater. Lett. 74 (2012) 176–179.
[14] F.Y. Cheng, J. Chen, J. Mater. Chem. 21 (2011) 9841–9848.
[15] F. Sauvage, V. Bodenez, H. Vezin, M. Morcrette, J.M. Tarascon, K.R. Poeppelmeier, J. Power Sourc. 195 (2010) 1195–1201.
[16] E.S. Takeuchi, W.C. Thiebolt, J. Electrochem. Soc. 135 (1988) 2691–2694.
[17] N. Zhou, Y.Y. Liu, J.G. Li, E. Uchaker, S.Q. Liu, K.L. Huang, G.Z. Cao, J. Power Sourc. 213 (2012) 100–105.
[18] L.F. Shen, X.G. Zhang, E. Uchaker, C.Z. Yuan, G.Z. Cao, Adv. Energy Mater. 2 (2012) 691–698.
[19] A.Q. Pan, D.W. Liu, X.Y. Zhou, B.B. Garcia, S.Q. Liang, J. Liu, G.Z. Cao, J. Power Sourc. 195 (2010) 3893–3899.
[20] A.Q. Pan, J. Liu, J.G. Zhang, G.Z. Cao, W. Xu, Z.M. Nie, X.A. Jie, D.W. Choi, B.W. Arey, C.M. Wang, S.Q. Liang, J. Mater. Chem. 21 (2011) 1153–1161.
[21] R.A. Leising, E.S. Takeuchi, Chem. Mater. 6 (1994) 489–495.
[22] R.A. Leising, W.C. Thiebolt, E.S. Takeuchi, Inorg. Chem. 33 (1994) 5733–5740.
[23] A.Q. Pan, J.G. Zhang, G.Z. Cao, S.Q. Liang, C.M. Wang, Z.M. Nie, B.W. Arey, W. Xu, D.W. Liu, J. Xiao, G.S. Li, J. Liu, J. Mater. Chem. 21 (2011) 10077–10084.
[24] A.Q. Pan, J. Liu, J.G. Zhang, W. Xu, G.Z. Cao, Z.M. Nie, B.W. Arey, S.Q. Liang, Electrochem. Commun. 12 (2010) 1674–1677.
[25] G. Pistoia, M. Pasquali, G. Wang, L. Li, J. Electrochem. Soc. 137 (1990) 2365.
[26] R. Tossici, R. Marassi, M. Berrettoni, S. Stizza, G. Pistoia, Solid State Ionics 57 (1992) 227.
[27] Q.L. Bao, S.J. Bao, C.M. Li, X. Qi, C.T. Pan, J.F. Zang, W.L. Wang, D.Y. Tang, Chem. Mater. 19 (2007) 5965–5972.